Inorg. Chem. **2003**, *42*, 5932–5937

Investigation of the Spin Exchange Interactions and Magnetic Structures of the $CrVO_4$-Type Transition Metal Phosphates, Sulfates, and Vanadates by Spin Dimer Analysis

H.-J. Koo and M.-H. Whangbo*

Department of Chemistry, North Carolina State University, Raleigh, North Carolina 27695-8204

K.-S. Lee

Department of Chemistry, The Catholic University of Korea, Puchon, Kyunggi-Do, South Korea 422-743

Received March 31, 2003

The $CrVO_4$-type magnetic oxides $MM'O_4$ consist of edge-sharing MO_4 octahedral chains condensed with $M'O_4$ tetrahedra and exhibit a wide variety of magnetic structures. The magnetic properties of these oxides were examined by studying their spin exchange interactions on the basis of spin dimer analysis. The nature and magnitudes of the intra- and interchain spin exchange interactions depend on the square-to-rectangle distortion in the basal planes of the MO_4 chain and on the difference between the M 3d and O 2p orbital energies. The spiral magnetic structures of β-$CrPO_4$ and $MnSO_4$ originate from the pseudohexagonal arrangement of the MO_4 chains and the frustrated interchain antiferromagnetic interactions.

Introduction

The crystal structures and magnetic properties of the $CrVO_4$-type solids have been studied over the past 50 years.[1] These oxides include phosphates $TiPO_4$,[2−6] VPO_4,[2−4,6] β-$CrPO_4$,[2,7,8] and $FePO_4$-II,[9] sulfates $MnSO_4$,[10−12] $FeSO_4$,[12] $CoSO_4$,[12] and $NiSO_4$,[12] and vanadates $CrVO_4$[12,13] and $FeVO_4$-II.[14] The structural building blocks of these magnetic oxides $MM'O_4$ are MO_6 octahedra (M = Ti, V, Cr, Mn, Fe, Ni) and $M'O_4$ tetrahedra (M′ = P, S, V). The MO_6 octahedra share their trans edges to form MO_4 chains (Figure 1a), in which there are two types of oxygen atoms (i.e., O_{eq} and O_{ax}). Each $M'O_4$ tetrahedron is condensed with three adjacent MO_4 chains such that one O−O edge is represented by two adjacent O_{ax} atoms of one MO_4 chain and the opposite O−O edge by the O_{eq} atoms of the remaining two MO_4 chains (one O_{eq} from each chain) (Figure 1b). As a consequence, the MO_4 chains have a pseudohexagonal arrangement (Figure 1c).

The $CrVO_4$-type oxides exhibit a wide spectrum of magnetic properties despite their structural similarity, as summarized in Table 1. The magnetic susceptibility vs temperature (χ-vs-T) curves of VPO_4, β-$CrPO_4$, $CrVO_4$, and $FeVO_4$-II exhibit a broad maximum (χ_{max}) expected for a one-dimensional (1D) Heisenberg antiferromagnetic (AFM) chain.[15] The intrachain magnetic order is AFM in VPO_4,

* To whom correspondence should be addressed. E-mail: mike_whangbo@ncsu.edu

(1) For a recent review, see: Baran, E. J. *J. Mater. Sci*. **1998**, *33*, 2479.
(2) Yamauchi, T.; Ueda, Y. *J. Magn. Magn. Mater*. **1998**, *177*−*181*, 705.
(3) Glaum, R.; Reehuis, M.; Stüsser, N.; Kaiser, U.; Reinauer, F. *J. Solid State Chem.* **1996**, *126*, 15.
(4) Glaum, R.; Gruehn, R. *Z. Kristallogr*. **1992**, *198*, 41.
(5) Leclaire, A.; Benmoussa, A.; Borel, M. M.; Grandin, A.; Raveau, B. *Eur. J. Solid State Inorg. Chem.* **1991**, *28*, 1323.
(6) Kinomura, N.; Muto, F.; Koizumi, M. *J. Solid State Chem*. **1982**, *45*, 252.
(7) Wright, J. P.; Attfield, J. P.; David, W. I. F.; Forsyth, J. B. *Phys. Rev. B* **2000**, *62*, 992.
(8) Attfield, J. P.; Battle, P. D.; Cheetham, A. K. *J. Solid State Chem*. **1985**, *57*, 357.
(9) Battle, P. D.; Gibb, T. C.; Hu, G.; Munro, D. C.; Attfield, J. P. *J. Solid State Chem*. **1986**, *65*, 343.
(10) Lecomte, M.; de Gunzbourg, J.; Teyrol, M.; Miedan-Gros, A.; Allain, Y. *Solid State Commun*. **1972**, *10*, 235.
(11) Will, G.; Frazer, B. C.; Shirane, G.; Cox, D. E.; Brown, P. J. *Phys. Rev. B* **1965**, *140*, A2139.
(12) Frazer, B. C.; Brown, P. J. *Phys. Rev. B* **1962**, *125*, 1283.
(13) Isasi, M. J.; Sáez,-Puche, R.; Veiga, M. L.; Pico, C.; Jerez, A. *Mater. Res. Bull*. **1988**, *23*, 595.
(14) Oka, Y.; Yao, T.; Yamamoto, N.; Ueda, Y.; Kawasaki, S.; Azuma, M.; Takano, M. *J. Solid State Chem*. **1996**, *123*, 54.
(15) Kahn, O. *Molecular Magnetism*; VCH Publishers: Weinheim, Germany, 1993.

10.1021/ic030115e CCC: $25.00
Published on Web 08/21/2003

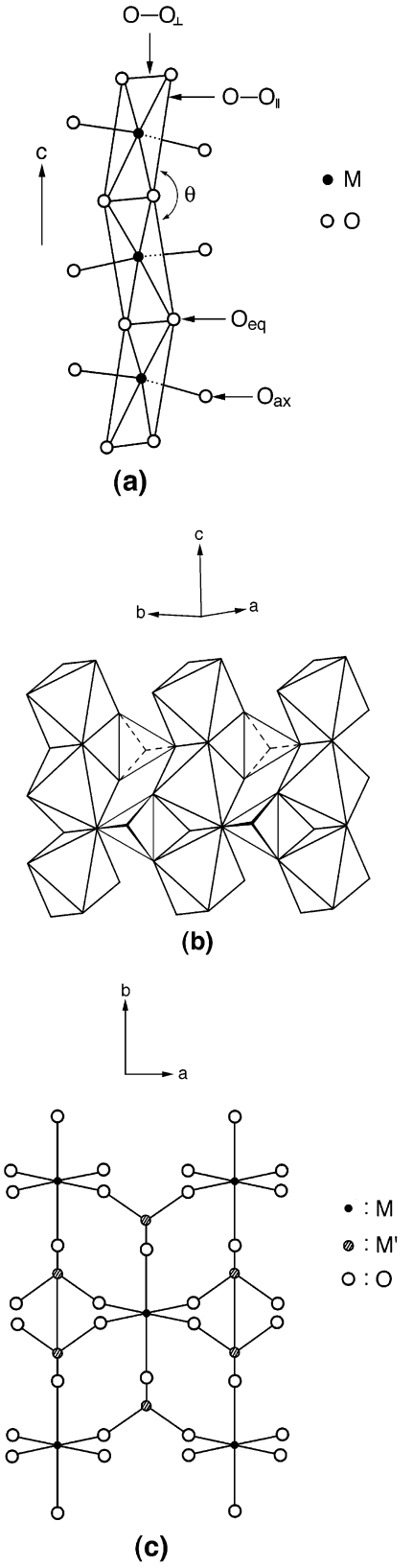

Figure 1. Crystal structure of the $CrVO_4$-type oxides $MM'O_4$: (a) perspective view of an MO_4 chain that is made up of trans edge-sharing MO_6 octahedra; (b) polyhedral view of how the MO_4 chains are condensed with the $M'O_4$ tetrahedra; (c) projection view of the MO_4 chains and $M'O_4$ tetrahedra along the chain direction.

β-$CrPO_4$, $FePO_4$-II, $MnSO_4$, and $CrVO_4$, while it is ferromagnetic (FM) in $FeSO_4$, $CoSO_4$, and $NiSO_4$. The interchain magnetic order is FM in $CrVO_4$, is spiral in β-$CrPO_4$ and $MnSO_4$, and is AFM in VPO_4, $FePO_4$-II, $FeSO_4$, $CoSO_4$, and $NiSO_4$. So far, no explanation has been provided for why the $CrVO_4$-type oxides exhibit such diverse magnetic properties. To understand the magnetic properties of these oxides, it is necessary to analyze their spin exchange interactions. In this work, we probe this question by performing spin dimer analysis[16−21] on the basis of extended Hückel tight binding (EHTB) calculations.[22,23] This approach has been quite successful in understanding the spin exchange interactions and magnetic structures of numerous magnetic solids.[16−21]

Table 1. Magnetic Properties of the $CrVO_4$ Type Solids

	intrachain order	interchain order	general description
$TiPO_4$			temp-independent χ above 140 K[a]
			broad χ_{max} above room temp?[b]
			no long-range order down to 2 K[c]
VPO_4	AFM[c]	AFM[c]	broad χ_{max} around 140 K[a,c]
	$J/k_B = -102, -120$ K[b]	$J''/k_B = -0.2$ K[b]	
β-$CrPO_4$	AFM[d]	spiral[d,e]	broad χ_{max} around 40 K[a,d]
	$J/k_B = -19, -24$ K[b]	$J''/k_B = -0.7$ K[b]	
$FePO_4$-II	canted AFM[f]	AFM[f]	$T_N = 4.2$ K[f]
$MnSO_4$	AFM[g]	spiral[g]	$T_N = 11.5$ K[h]
$FeSO_4$	FM[i]	AFM[i]	$T_N = 21$ K[i]
$CoSO_4$	canted FM[i]	AFM[i]	$T_N = 15.5$ K[i]
$NiSO_4$	FM[i]	AFM[i]	$T_N = 37$ K[i]
$CrVO_4$	AFM[i]	FM[i]	broad χ_{max} around 75 K[j]
	$J/k_B = -25, -22$ K[j]		$T_N \approx 50$ K[i]
$FeVO_4$-II			broad χ_{max} around 52 K[k]
			3D ordering below 40 K[k]

[a] Reference 6. [b] Reference 2. [c] Reference 3. [d] Reference 7. [e] Reference 8. [f] Reference 9. [g] Reference 11. [h] Reference 10. [i] Reference 12. [j] Reference 13. [k] Reference 14.

Structural Parameters Important for Spin Exchange Interactions

In the $CrVO_4$-type oxides $MM'O_4$ (M = transition metal; M′ = P, S, V), the intrachain spin exchange interactions are of the superexchange (SE) type that takes place through the M−O−M paths, and the interchain spin exchange interactions are of the super-superexchange (SSE) type that takes place through the M−O···O−M paths. Thus, a spin dimer (i.e., a structural unit of a solid consisting of two spin sites) representing an SE interaction is given by an edge-sharing octahedral dimer M_2O_{10} (Figure 2a) and that representing an SSE interaction by a dimer M_2O_{12} made up of two isolated MO_6 octahedra (Figure 2b).

(16) For a recent review, see: Whangbo, M.-H.; Koo, H.-J.; Dai, D. *J. Solid State Chem.*, in press.
(17) Whangbo, M.-H.; Koo, H.-J.; Dai, D.; Jung, D. *Inorg. Chem.* **2002**, *41*, 5575.
(18) Koo, H.-J.; Whangbo, M.-H.; VerNooy, P. D.; Torardi, C. C.; Marshall, W. J. *Inorg. Chem.* **2002**, *41*, 4664.
(19) Whangbo, M.-H.; Koo, H.-J. *Inorg. Chem.* **2002**, *41*, 3570.
(20) Whangbo, M.-H.; Koo, H.-J.; Dumas, J.; Continentino, M. A. *Inorg. Chem.* **2002**, *41*, 2193.
(21) Koo, H.-J.; Whangbo, M.-H.; Lee, K.-S. *J. Solid State Chem.* **2002**, *169*, 143.
(22) Hoffmann, R. *J. Chem. Phys.* **1963**, *39*, 1397.
(23) Our calculations were carried out by employing the SAMOA (Structure and Molecular Orbital Analyzer) program package (Dai, D.; Ren, J.; Liang, W.; Whangbo, M.-H., http://chvamw.chem.ncsu.edu/, 2002).

Table 2. Structural Parameters of the $CrVO_4$-Type Magnetic Solids $MM'O_4$

	$M-O_{eq}$, $M-O_{ax}$ (Å)	$O-O_{\perp}$, $O-O_{\parallel}$ (Å)	R[a]	θ (deg)	O···O (Å) (along a)[b]	O···O (Å) (along $a+b$)[c]
$TiPO_4$[d]	2.119, 1.949	2.747, 3.227	0.851	159.1	2.552 (×2)	2.501 (×2)
VPO_4[d]	2.080, 1.928	2.681, 3.181	0.843	162.1	2.550 (×2)	2.497 (×2)
β-$CrPO_4$[e]	2.028, 1.926	2.625, 3.093	0.849	163.0	2.546 (×2)	2.503 (×2)
$MnSO_4$[f]	2.249, 2.108	2.840, 3.486	0.815	158.2	2.420 (×2)	2.379 (×2)
$NiSO_4$[g]	2.054, 1.967	2.578, 3.199	0.806	164.2	2.578 (×2)	2.593 (×2)
$CrVO_4$[g]	2.055, 1.946	2.817, 2.993	0.941	173.7	2.751 (×2)	2.874 (×2)
$FeVO_4$-II[h]	2.029, 2.006	2.649, 3.074	0.862	167.7	2.980 (×2)	2.809 (×2)

[a] R refers to the ratio $O-O_{\perp}/O-O_{\parallel}$. [b] Between O_{eq} and O_{eq}. [c] Between O_{eq} and O_{ax}. [d] Reference 4. [e] Reference 8 [f] Reference 11. [g] Reference 12. [h] Reference 14.

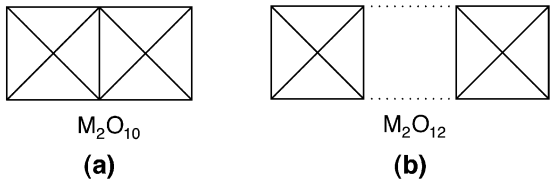

Figure 2. Projection polyhedral views of the spin dimers M_2O_{10} and M_2O_{12} that represent the SE and SSE interactions, respectively.

The structural parameters of $MM'O_4$ important for their SE and SSE interactions are listed in Table 2. These parameters were taken from the available crystal structures reported in the literature. It is noted that the $M-O_{eq}$ bond is longer than the $M-O_{ax}$ bond in each MO_4 chain. Each $M(O_{eq})_4$ unit of a MO_6 octahedron is rectangular in shape such that the O−O edge perpendicular to the chain (i.e., $O-O_{\perp}$) is shorter than that parallel to the chain (i.e., $O-O_{\parallel}$). The extent of the square-to-rectangle distortion in each $M(O_{eq})_4$ unit is measured by how small the ratio $R = O-O_{\perp}/O-O_{\parallel}$ is. The sulfates $MnSO_4$ and $NiSO_4$ have very small R values (Table 2). In a spin dimer M_2O_{10} representing an SE interaction (Figure 2a), the two $M(O_{eq})_4$ rectangles make a dihedral angle θ ranging from ∼160 to ∼170°. In a spin dimer M_2O_{12} representing an SSE interaction (Figure 2b), the two MO_6 octahedra have shorter O···O contacts along the $(a+b)$-direction than along the a-direction in all oxides except for $NiSO_4$ and $CrVO_4$ (Table 2). The O···O contacts of the vanadates $CrVO_4$ and $FeVO_4$-II are considerably longer compared with those of the other oxides. The $M(O_{eq})_4$ rectangles of a spin dimer M_2O_{12} are coplanar along the a-direction but not along the $(a+b)$-direction.

Spin Dimer Analysis

Physical properties of a magnetic solid are described in terms of a spin-Hamiltonian expressed as a sum of pairwise spin exchange interactions. In terms of first-principles electronic structure calculations the strengths of spin exchange interactions (i.e., spin exchange parameters J) are estimated on the basis of electronic structure calculations for spin dimers[16,24−26] or electronic band structure calculations for magnetic solids.[27,28] For magnetic solids with large and complex unit cell structures these quantitative methods become difficult to apply. In understanding the anisotropy of spin exchange interactions of magnetic solids, however, it is often sufficient to examine their relative magnitudes.[16−21] In general, a spin exchange parameter J is written as $J = J_F + J_{AF}$.[15,29] The FM term J_F (>0) is small so that the spin exchange becomes FM (i.e., $J > 0$) if the AFM term J_{AF} (<0) is negligibly small in magnitude, but becomes AFM (i.e., $J < 0$) if the J_{AF} term is large in magnitude. Consequently, qualitative trends in spin exchange interactions can be discussed by studying those in their J_{AF} terms.

When each spin site of a spin dimer has m unpaired spins, the overall spin exchange parameter J of the spin dimer is described by[30]

$$J = \frac{1}{m^2}\sum_{\mu=1}^{m}\sum_{\nu=1}^{m} J_{\mu\nu} \qquad (1)$$

From the viewpoint of nonorthogonal magnetic orbitals localized at the spin sites, the AFM contribution J_{AF} from each off-diagonal term $J_{\mu\nu}$ ($\mu \neq \nu$) is negligible because the overlap integral between two adjacent magnetic orbitals of different symmetry is either zero or negligible. Consequently, for an AFM spin exchange interactions J, only the diagonal $J_{\mu\mu}$ terms can contribute significantly. Thus, eq 1 can be approximated by

$$J \approx \frac{1}{m^2}\sum_{\mu=1}^{m} J_{\mu\mu} \qquad (2)$$

so that the associated AFM term J_{AF} can be written as[16,17,20,21,31]

$$J_{AF} \approx -\frac{\langle(\Delta e)^2\rangle}{U_{eff}} \qquad (3)$$

where U_{eff} is the effective on-site repulsion and $\langle(\Delta e)^2\rangle$ is the average of the spin−orbital interaction energy squares (see below).[32]

(24) Illas, F.; Moreira, I. de P. R.; de Graaf, C.; Barone, V. *Theor. Chem. Acc.* **2000**, *104*, 265 and references therein.
(25) Noodleman, L. *J. Chem. Phys.* **1981**, *74*, 5737.
(26) Dai, D.; Whangbo, M.-H. *J. Chem. Phys.* **2001**, *114*, 2887.
(27) Derenzo, S. E.; Klitenberg, M. K.; Weber, M. J. *J. Chem. Phys*. **2000**, *112*, 2074 and references therein.
(28) Korotin, M. A.; Anisimov, V. I.; Saha-Dasgupta, T.; Dasgupta, I. *J. Phys.: Condens. Matter* **2000**, *12*, 113.
(29) Hay, P. J.; Thibeault, J. C.; Hoffmann, R. *J. Am. Chem. Soc*. **1975**, *97*, 4884.
(30) Charlot, M. F.; Kahn, O. *Nouv. J. Chim*. **1980**, *4*, 567.
(31) Dai, D.; Koo, H.-J.; Whangbo, M.-H. In *Solid State Chemistry of Inorganic Materials III*; MRS Symposium Proceedings Vol. 658; Geselbracht, M. J., Greedan, J. E., Johnson, D. C., Subramanian, M. A., Eds.; Materials Research Society: Warrendale, PA, 2001; GG5.3.1−5.3.11 and references therein.
(32) This expression is valid when spin exchange parameters of a spin Hamiltonian are written as J instead of $2J$.

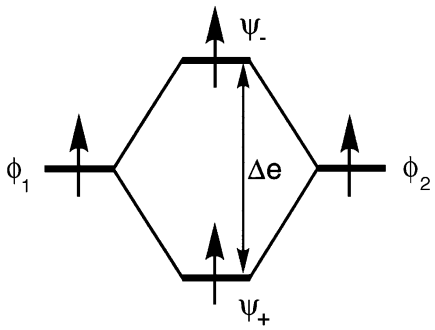

Figure 3. Spin−orbital interaction energy Δe of a spin dimer with two equivalent spin sites.

In the case of the $CrVO_4$-type oxides $MM'O_4$, the unpaired spins reside in the d-block levels of the MO_6 octahedra. If a spin site has the $(t_{2g})^3(e_g)^2$ configuration, the $\langle(\Delta e)^2\rangle$ value is given by

$$\langle(\Delta e)^2\rangle = \frac{1}{m^2}\sum_{\mu=1}^{m}(\Delta e_{\mu\mu})^2 \qquad (4)$$

where $\Delta e_{\mu\mu}$ is the spin−orbital interaction energy associated with the magnetic orbitals ϕ_μ of the two spin sites ($\mu = 1-3$ for the t_{2g} levels and $\mu = 4-5$ for the e_g levels) (Figure 3). In general, the total number of unpaired spins m at a spin site can be divided into the m_t and m_e unpaired spins in the t_{2g}- and e_g-block levels, respectively (i.e., $m = m_t + m_e$). ($m_t = 1$ and $m_e = 0$ for $TiPO_4$; $m_t = 2$ and $m_e = 0$ for VPO_4; $m_t = 3$ and $m_e = 0$ for β-$CrPO_4$ and $CrVO_4$; $m_t = 3$ and $m_e = 2$ for $MnSO_4$ and $FeVO_4$-II; $m_t = 0$ and $m_e = 2$ for $NiSO_4$.) If we define the following energy terms

$$(\Delta e_{t2g})^2 = (\Delta e_{11})^2 + (\Delta e_{22})^2 + (\Delta e_{33})^2$$

$$(\Delta e_{eg})^2 = (\Delta e_{44})^2 + (\Delta e_{55})^2 \qquad (6)$$

then the $\langle(\Delta e)^2\rangle$ value can be approximated by[16,20]

$$\langle(\Delta e)^2\rangle \approx \frac{1}{m^2}\left[\frac{m_t}{3}\frac{m_t}{3}(\Delta e_{t2g})^2 + \frac{m_e}{2}\frac{m_e}{2}(\Delta e_{eg})^2\right] \qquad (7)$$

It is important to note that the $\langle(\Delta e)^2\rangle$ value becomes smaller when a spin site has a large number of unpaired spins (i.e., large m).

In describing the spin exchange interactions of magnetic solids in terms of Δe values obtained from EHTB calculations, it is necessary[16−21,31] to employ double-ζ Slater type orbitals[33] for both the 3d orbitals of the transition metal and the s/p orbitals of the surrounding ligand atoms. The atomic orbital parameters of M and O employed for our calculations are summarized in Table 3.

Results and Discussion

The $\langle(\Delta e)^2\rangle$ values of $MM'O_4$ calculated for the intrachain spin exchange path (J_{intra}) and for the interchain spin exchange paths along the a- and $(a + b)$-directions (J_a and J_{a+b}, respectively) are listed in Table 4. In each compound the relative values of $\langle(\Delta e)^2\rangle$ are given with respect to the largest one. In all $MM'O_4$ except for $NiSO_4$, the strongest AFM interaction is found for the intrachain spin exchange, in good agreement with the available experimental results (Table 1). This explains why many of these oxides exhibit a broad maximum in their χ-vs-T curves as if they are 1D Heisenberg AFM chain systems. For $NiSO_4$, the strongest AFM interaction is found for the interchain spin exchange interaction J_a while the intrachain AFM interaction is absent. The latter agrees with the fact that the intrachain spin exchange is FM in $NiSO_4$. Note that the intrachain AFM interaction is quite strong in $TiPO_4$. This is consistent with the observation that the magnetic susceptibility of $TiPO_4$ is nearly independent of temperature above 140 K.

Spiral magnetic structures can arise when spin exchange interactions are frustrated and are dominant over the single ion anisotropy.[7] In β-$CrPO_4$, the interchain AFM interactions J_a and J_{a+b} are not negligible compared with the intrachain AFM interaction. Thus, given the triangular arrangement of the MO_4 chains (Figure 1c), the interchain AFM interactions will be frustrated.[7,15] Since the interchain AFM interactions J_a and J_{a+b} are quite similar in magnitude, the interchain AFM interactions will have the cycloidal spiral structure with the propagation vector of approximately $3a_0$ (Figure 4),[7]

Table 3. Exponents ζ_i and Valence Shell Ionization Potentials H_{ii} of Slater-Type Orbitals χ_i Used for Extended Hückel Tight-Binding Calculations[a]

atom	χ_i	H_{ii} (eV)	ζ_i	C[b]	ζ'_i	C'[b]
Ti	4s	−8.97	1.619	1.00		
Ti	4p	−5.44	1.200	1.00		
Ti	3d	−10.81	4.67	0.3646	1.986	0.7556
V	4s	−8.81	1.697	1.00		
V	4p	−5.52	1.260	1.00		
V	3d	−11.00	5.052	0.3738	2.173	0.7456
Cr	4s	−8.66	1.772	1.00		
Cr	4p	−5.24	1.300	1.00		
Cr	3d	−11.22	5.410	0.3830	2.340	0.7367
Mn	4s	−9.75	1.844	1.00		
Mn	4p	−5.89	1.350	1.00		
Mn	3d	−11.67	5.767	0.3898	2.510	0.7297
Fe	4s	-9.10	1.925	1.00		
Fe	4p	−5.32	1.390	1.00		
Fe	3d	−12.60	6.068	0.4038	2.618	0.7198
Ni	4s	−9.17	2.077	1.00		
Ni	4p	−5.15	1.470	1.00		
Ni	3d	−13.49	6.706	0.4212	2.874	0.7066
O	2s	−32.3	2.688	0.7076	1.675	0.3745
O	2p	−14.8	3.694	0.3322	1.659	0.7448

[a] H_{ii}'s are the diagonal matrix elements $\langle\chi_i|H^{eff}|\chi_i\rangle$, where H^{eff} is the effective Hamiltonian. In our calculations of the off-diagonal matrix elements $H^{eff} = \langle\chi_i|H^{eff}|\chi_j\rangle$, the weighted formula was used. See: Ammeter, J.; Bürgi, H.-B.; Thibeault, J.; Hoffmann, R. *J. Am. Chem. Soc.* **1978**, *100*, 3686. [b] Contraction coefficients used in the double-ζ Slater-type orbital.

Table 4. $\langle(\Delta e)^2\rangle$ Values Calculated for the Intra- and Interchain Spin Exchange Paths of the $CrVO_4$-Type Magnetic Solids[a]

	J_{intra}	J_a	J_{a+b}
$TiPO_4$	3080(1.00)	290(0.09)	170(0.05)
VPO_4	1000(1.00)	10(0.01)	170(0.17)
β-$CrPO_4$	800(1.00)	180(0.23)	200(0.25)
$MnSO_4$	240(1.00)	60(0.24)	40(0.16)
$NiSO_4$	0(0.00)	3710(1.00)	240(0.07)
$CrVO_4$	2330(1.00)	70(0.03)	110(0.05)
$FeVO_4$-II	1340(1.00)	50(0.04)	50(0.04)

[a] $\langle(\Delta e)^2\rangle$ values are in units of $(meV)^2$.

(33) Clementi, E.; Roetti, C. *At. Data Nuclear Data Tables* **1974**, *14*, 177.

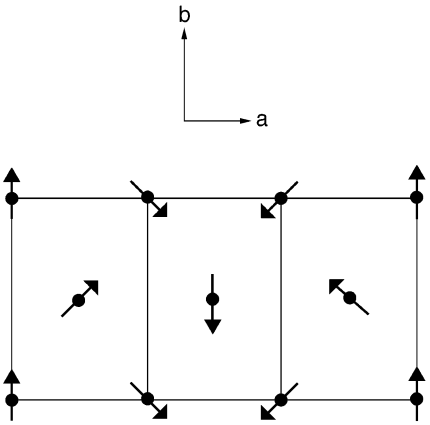

Figure 4. Cycloidal spiral magnetic structure observed for β-$CrPO_4$, where each heavy dot represents an antiferromagnetically ordered CrO_4 chain.

Table 5. Variation of the $\langle(\Delta e)^2\rangle$ Values Calculated for the Intra- and Interchain Spin Exchange Paths of $NiSO_4$ as a Function of the Ratio $R = O{-}O_\perp/O{-}O_{||}$[a]

$O{-}O_\perp$ (Å)	$O{-}O_{||}$ (Å)	R	J_{intra}	J_a
2.578	3.199	0.806	0	3710
2.688	3.088	0.870	360	3480
2.788	2.988	0.933	1540	3530
2.888	2.888	1.000	3400	3670

[a] $\langle(\Delta e)^2\rangle$ values are in units of $(meV)^2$.

where a_0 is the a-parameter of the chemical cell. This accounts for the experimental observation of the cycloidal spiral structure with the propagation vector of $3.07a_0$.[8] $MnSO_4$ has a spiral magnetic structure in which the propagation vector is approximately $6a_0$.[11] This observation is understandable because the interchain AFM interactions J_a and J_{a+b} are not negligible compared with the intrachain AFM interaction J_{intra} and because one interchain AFM interaction is stronger than the other interchain AFM interaction (i.e., $J_a/J_{a+b} \approx 3/2$).

The intrachain spin exchange is FM in the sulfate $NiSO_4$ (Table 1). As noted from Table 2, the square-to-rectangle distortion of the $M(O_{eq})_4$ unit is strongest in the sulfate $NiSO_4$. To examine how this distortion affects the relative strengths of the intrachain interaction J_{intra} and the interchain interaction J_a, we construct several hypothetical structures of the $Ni(O_{eq})_4$ unit by gradually changing the $O{-}O_\perp$ and $O{-}O_{||}$ lengths toward a square structure under the condition that the sum of the $O{-}O_\perp$ and $O{-}O_{||}$ lengths remains constant. Then we calculate the $\langle(\Delta e)^2\rangle$ values for the exchange paths J_{intra} and J_a while keeping the O···O distances along the a-direction at 2.578 Å as found for the real structure. Results of these calculations, summarized in Table 5, reveal that the intrachain AFM interaction J_{intra} is nearly as strong as the interchain AFM interaction J_a when the $Ni(O_{eq})_4$ unit is square and that the interchain AFM interaction J_a is hardly affected by the square-to-rectangle distortion whereas the intrachain AFM interaction J_{intra} is strongly diminished as the square-to-rectangle distortion proceeds. Therefore, in $NiSO_4$, the square-to-rectangle distortion is critical for why the intrachain AFM interaction is absent so that the intrachain spin exchange becomes FM. The extent of the square-to-rectangle distortion in $MnSO_4$ is only slightly greater than that in $NiSO_4$ (i.e., $R = 0.815$ vs 0.806). This explains why the intrachain AFM interaction is not strong in $MnSO_4$. One should recall that the strength of the intrachain AFM interaction is also governed by an electronic factor, namely, it becomes reduced as the energy difference between the M 3d and O 2p levels is decreased (equivalently, as the M 3d orbital becomes more contracted). Thus, it is understandable that the intrachain spin exchange is FM in $FeSO_4$ and $CoSO_4$ (Table 1). This electronic factor also accounts for why the intrachain AFM interactions of the phosphates MPO_4 (M = Ti, V, Cr), which have electrons only in the t_{2g}-block levels, decrease their strengths in the order $TiPO_4 > VPO_4 > \beta$-$CrPO_4$ (Table 4).

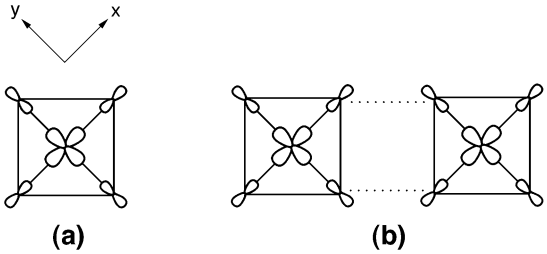

Figure 5. (a) e_g-block magnetic orbital based on the 3d x^2-y^2 orbital. (b) SSE interaction between two such magnetic orbitals.

Finally, we discuss the reason why the interchain spin exchange is AFM in the sulfate $NiSO_4$ and its implications. Figure 5a depicts one of the e_g-block orbitals of the NiO_6 octahedron, in which the Ni 3d x^2-y^2 orbital is combined out-of-phase with the O 2p orbitals. As illustrated in Figure 5b, the strength of the interchain AFM interaction J_a resulting from such a magnetic orbital increases with increasing the overlap between the 2p orbitals in the short O···O contacts.[16,18] The magnitude of this overlap increases with increasing the weight of the O 2p orbital in the magnetic orbital. In general, the M 3d level lies higher than the O 2p level for early transition metal atoms and becomes closer to the O 2p level for late transition metal atoms. With decrease of the energy difference between the M 3d and O 2p levels, the weight of the O 2p orbitals in the magnetic orbitals of an MO_6 octahedron (i.e., either the t_{2g}- or e_g-block orbitals) should increase.[34] Thus, the weight of the O 2p orbitals is large for NiO_6 and should decrease gradually on going from NiO_6 to CoO_6 to FeO_6 and MnO_6. This explains why the interchain spin exchange J_a is strongly AFM in $NiSO_4$ but becomes weakly AFM in $MnSO_4$.

Concluding Remarks

The magnetic structures of the $CrVO_4$-type oxides $MM'O_4$ are well accounted for in terms of the relative J_{AF} values calculated for the intra- and interchain spin exchange paths using spin dimer analysis. In all $MM'O_4$ except for $NiSO_4$, the strongest AFM interaction is found for the intrachain spin exchange. The occurrence of the spiral magnetic structures in β-$CrPO_4$ and $MnSO_4$ is explained by the facts that the MO_4 chains have a pseudohexagonal arrangement and that the interchain AFM interactions J_a and J_{a+b} are similar in

(34) Albright, T. A.; Burdett, J. K.; Whangbo, M.-H. *Orbital Interactions in Chemistry*; Wiley: New York, 1985.

strength and are not negligible compared with the intrachain AFM interaction J_{intra}. The square-to-rectangle distortion of the $M(O_{eq})_4$ unit is strong in the sulfate $NiSO_4$ and as a result diminishes the intrachain AFM interaction so that the intrachain spin exchange of $NiSO_4$ is FM. The weight of the O 2p orbitals in the magnetic orbitals is large for NiO_6, so that the interchain spin exchange J_a is strongly AFM in $NiSO_4$. The weight of the O 2p orbitals in the magnetic orbitals becomes smaller on going from NiO_6 to MnO_6, so that the interchain spin exchange J_a becomes weakly AFM in $MnSO_4$.

Acknowledgment. The work at North Carolina State University was supported by the Office of Basic Energy Sciences, Division of Materials Sciences, U.S. Department of Energy, under Grant DE-FG02-86ER45259. K.-S.L. thanks The Catholic University of Korea for Grant 2003.

IC030115E